

Research Article

Role of Interface in Multilayered Composites under Irradiation: A Mathematical Investigation

Jaime Ortún-Palacios,^{1,2} Antonio Mario Locci,³ Sarah Fadda,^{3,4}
Francesco Delogu,³ and Santiago Cuesta-López^{1,2}

¹International Research Centre in Critical Raw Materials (ICCRAM), University of Burgos, Plaza Misael Bañuelos s/n, 09001 Burgos, Spain

²Advanced Materials, Nuclear Technology and Applied Bio/Nanotechnology, Consolidated Research Unit UIC-154, Castilla y León, Spain

³Dipartimento di Ingegneria Meccanica, Chimica e dei Materiali, Università degli Studi di Cagliari, Via Marengo 2, 09123 Cagliari, Italy

⁴Centre for Process Systems Engineering, Department of Chemical Engineering, Imperial College London, London SW7 2AZ, UK

Correspondence should be addressed to Antonio Mario Locci; antonio.locci@dimcm.unica.it

Received 27 July 2017; Accepted 1 October 2017; Published 31 October 2017

Academic Editor: Fantao Kong

Copyright © 2017 Jaime Ortún-Palacios et al. This is an open access article distributed under the Creative Commons Attribution License, which permits unrestricted use, distribution, and reproduction in any medium, provided the original work is properly cited.

A continuum model of point-defects evolution during irradiation of a multilayer composite material is presented in this work. Nonstationary balance equations are used to describe production, recombination, transport, and annihilation, or removal, of vacancies and interstitials in a β - α - β three-layer system (α = Cu and β = Nb, V, or Ni). In addition, transport and trapping of point-defects at interfaces are taken into account. Numerical investigation on similarities and differences between Cu/Nb, Cu/V, and Cu/Ni systems is also performed. A general comparison of model results reveals that average vacancy concentration is typically higher than SIA one in both layers for all the systems investigated. This is a consequence of the higher diffusion rate of SIAs with respect to vacancies. Stationary state is reached without saturating interface point-defect traps by all systems but Cu/Ni for the case of SIAs. It can be also seen that Cu/Nb and Cu/V systems have a very similar behavior regarding point-defect temporal evolution in copper (layer α), while higher SIA concentration at steady state is shown therein by the Cu/Ni structure. Moreover, Cu/V system displays the lower stationary vacancy concentration in layer β .

1. Introduction

Components of nuclear power systems will be exposed to aggressive environments of unprecedented magnitude consisting of irradiation, high temperatures, and corrosive fluids [1, 2]. Therefore, performances of materials in these conditions must be significantly improved to extend reliability, lifetime, and efficiency of future nuclear reactors [3] such as fast fission reactors [4, 5] and fusion reactors [6, 7]. In fact, materials degradation during exposure to irradiation environments imposes substantial safety and economic impediments to the development of nuclear reactors [8]. This is true also for the core of the actual nuclear reactors generation, which presents exceptionally stringent requirements for structural materials due to the combination of high

temperature, high stresses, a chemically aggressive coolant, and intense radiation fluxes as well as its need for unflinching mechanical integrity [3, 9].

Detrimental long-term evolution of materials under particle irradiation is largely due to the production of sustained net fluxes of point-defects (i.e., vacancies and interstitials) [3, 10]. The origin of these fluxes is the supersaturation of point-defects produced by irradiation, which is only partially diminished by recombination. Moreover, both the production and elimination of freely migrating point-defects are spatially biased so that vacancies and interstitials become separated [10]. In nuclear reactor environments, damage is also introduced by helium from transmutation reactions during high-energy neutron irradiation [11, 12]. In particular, helium is a byproduct of nuclear reactions that create α

particles (He nuclei) [13, 14]. Due to extremely low solubility and fast diffusion in metals, He atoms can easily migrate and combine with radiation-induced vacancies to precipitate into clusters or bubbles [15]. Moreover, He-ion irradiation into metals will generate vacancies and nearby self-interstitial defects [16].

The damaging effects on the mechanical and thermal properties of materials by the formation of He bubbles and point-defect clusters (e.g., voids) have received considerable attention in structural materials working in high radiation environments [16, 17]. Indeed, these nonequilibrium defects frequently lead to undesirable microstructural evolutions such as embrittlement, hardening, and dimensional as well as chemical instability of both structural and fuel components [11, 14]. Furthermore, swelling, solute redistribution, and creep are particularly troublesome in reactor materials subjected to neutron bombardment [18, 19]. Eventually surface deterioration phenomena such as spallation [20], swelling [2, 21], and blistering, which may cause wall erosion [15, 22], flaking of metal surfaces [23], and corrosion [8], may be observed [14, 21].

Extending performances, operating limits, reliability, efficiency, and lifetimes of present and future nuclear reactors thus requires the ability to remove radiation-induced point-defects and to mitigate the effects of He implantation on irradiated-material properties [11, 12]. Furthermore, candidate materials for nuclear applications must possess high strength and thermal stability in addition to excellent irradiation tolerance. However, these properties are difficult to realize simultaneously in one material because of apparently intrinsic tradeoffs between them [24]. This challenge calls then for novel approaches to design materials or special structures that resist radiation damage while maintaining high strength and toughness [3, 17].

In principle, a simple and direct approach to avoid the above deleterious microstructural changes can be realized if a high density of unbiased irradiation-induced point-defect sinks or traps can be introduced into the specimen [10]. This way, point-defects are absorbed and annihilated by enhanced Frenkel-pair recombination [8, 25] before they aggregate into clusters [17, 26].

These efforts include controlling the volume fraction and size distribution of solutes, precipitates, and interfaces with emphasis on optimizing both Frenkel-pair recombination rate and stability of the microstructure [10, 19]. Indeed, surfaces, grain boundaries, and interphase boundaries are sinks for radiation-induced point-defects and traps for implanted species such as helium [27, 28].

Nanostructured materials have recently gained much attention for these purposes as they present high densities of interphase or grain boundaries as sinks [19, 29]. Due to a large excess-free volume of interface (and grain boundaries) and higher diffusivity of defects along interfaces [11], vacancies and interstitials are likely to be annihilated after being attracted to the interfaces. It also appears that reducing microstructural dimensions increases radiation resistance because it shortens the average diffusion distance of point-defects to interfaces. Indeed, several types of nanocomposites have exhibited remarkable resistance to radiation and promise to

offer high resistance to radiation damage accumulation [28, 30], motivating research into potential uses of nanocomposite structural materials in future fission and fusion reactors [2].

One of the difficulties with this strategy has been maintaining the high densities of these traps/sinks during prolonged irradiation, particularly at very high temperatures, owing to such processes as radiation-induced (or enhanced) segregation, precipitation, and grain growth. [31]. In fact, nanocrystalline materials have high strength and improved radiation resistance [32] because of their high density of grain boundaries, which are sinks for irradiation-induced defects [24]. Nevertheless, most nanocrystalline materials are not thermally stable and coarsen rapidly even at modest temperatures [24, 33].

Efforts to engineer alloys tolerant to prolonged exposure to energetic particle irradiation have focused in recent years on multilayer films as a new concept of high densities of interfaces to provide sinks for point-defect annihilation and external species traps. Indeed, multiphase nanostructured materials such as nanolaminates could provide advanced radiation tolerance in comparison to traditional single phase bulk materials [8, 34].

Multilayer or nanolamellar composites have attracted much attention over the past decades due to their improved mechanical properties [35, 36]. Nanolayered composites can also be designed to produce ultrahigh strengths and enhanced radiation damage tolerance via tailoring of length scales to take advantage of the atomic structure and energetics of interfaces in order to provide the most effective sites for point-defect trapping and annihilation [3]. Indeed, the layered geometry with flat interfaces extending throughout the sample thickness may provide a benefit in this regard as compared to equiaxed-grain metals that may rapidly coarsen under irradiation at elevated temperatures [3]. Studies have shown that certain multilayer systems may significantly reduce radiation-induced damage in metallic materials [7, 34]. Moreover, heterophase interfaces in multilayer systems have also been shown to be effective sinks for radiation-induced defects with respect to grain boundaries [34, 37].

Therefore, multilayers with enhanced resistance to radiation can be potentially used in nuclear reactors as radiation protective coatings or fuel pin clad [37]. They may also provide additional parameters for materials design, beyond grain size and composition alone, which may be used to obtain properties that are not simultaneously achievable in a single material otherwise [34]. However, the advantages for radiation tolerance are not realized until the relevant length scale, such as the layer thickness, is reduced to the nanometer range. It appears then that the enhanced radiation damage tolerance in nanocomposites is a consequence of short diffusion distance to the nearest sink. At the smallest sizes in the layered composites of a few nanometers, diffusion distance to sinks are short enough, due to the huge interface area in the material, to enable rapid removal of point-defects before they can form into relatively stable aggregates [28]. Of course, the geometry of the nanolayered composite materials must be stable under the extreme irradiation conditions [3]. Moreover, chemical and microstructural stability of interfaces are also necessary factors. On the other hand, energy deposited

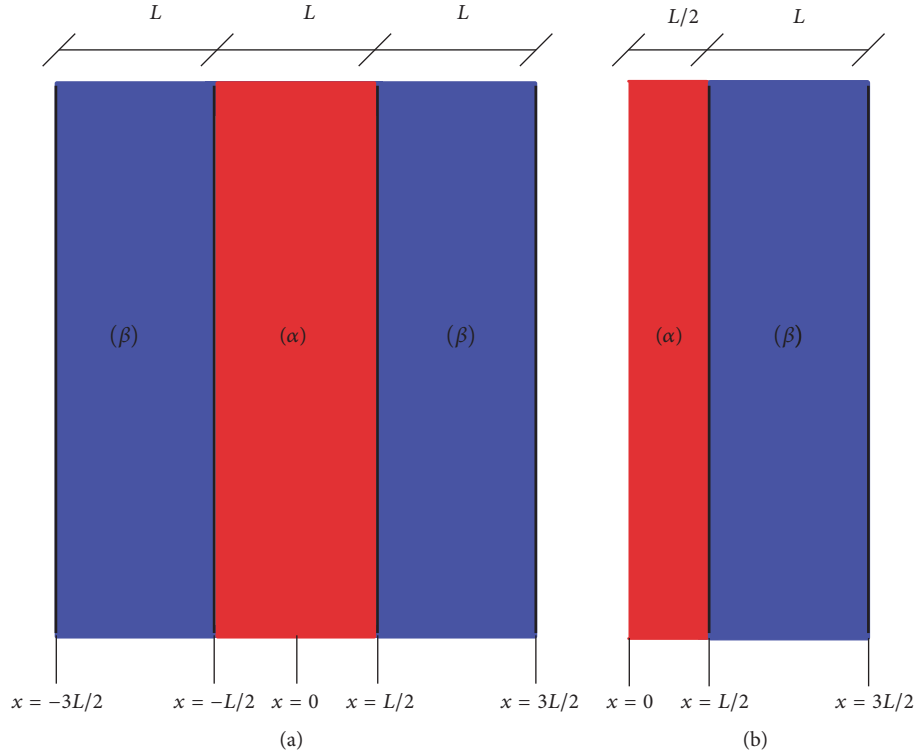


FIGURE 1: Schematic of (a) the entire system and (b) the half-symmetric part modelled. Layer α represents copper while β indicates niobium, nickel, or vanadium.

by incoming neutrons or ions may lead to extensive intermixing across interfaces, promoting morphological instabilities in these materials [28].

Several techniques as density functional theory (DFT), molecular dynamics, and phase field calculations were used to study the mechanisms underlying point-defect annihilation at interfaces of nanostructured metallic multilayer composites (NMMCs). This covered atomistic scale in enough detail. However, the overall mechanistic situation remained largely unknown. In this context, it is highly desirable to develop a continuum approach that describes long-term evolution of point-defects in NMMCs subjected to irradiation.

In order to provide a contribution along this line, Fadda et al. [38] modelled the dynamic behavior of vacancies and interstitials in continuum scale. They used nanostructured metallic monolayers of Cu and Nb as case study. A continuum spatial distribution of sinks either neutral or variable-biased was used to describe interfaces. This enables modelling grain boundaries and incoherent precipitates, that is, noncoherent interfaces, as neutral sinks, and coherent precipitates, that is, coherent interfaces, as variable-biased sinks [39]. Production, recombination, transport, and annihilation of point-defects at interfaces were defined by means of nonstationary balance equations. The effect of variation in layer thickness, temperature, production rate of point-defects, and surface recombination coefficient on annihilation processes at interfaces was studied. The present work focuses on modifying the model mentioned above to take into account surface characteristics deriving from coupling different metals. To

this end, boundary equations have been modified according to β - α - β NMMC scheme ($\alpha = \text{Cu}$ and $\beta = \text{Nb, Ni, or V}$) and the temporal evolution of point-defects concentration investigated. Numerical investigations on similarities and differences between Cu/Nb, Cu/Ni, and Cu/V systems have been also performed.

2. Mathematical Model

Let us consider the system depicted in Figure 1(a) where a layer of metal α is in between two layers of metal β [40]. The evolution of point-defect, that is, vacancy (v), and self-interstitial atom (SIA) (i) concentrations in layers α and β is described by the following one-dimensional spatial reaction-diffusion equations:

$$\frac{\partial C_j^{(\gamma)}}{\partial t} - D_j^{(\gamma)} \frac{\partial^2 C_j^{(\gamma)}}{\partial x^2} = K_0^{(\gamma)} - R_C^{(\gamma)} \quad j = i, v; \quad \gamma = \alpha, \beta, \quad (1)$$

along with their initial conditions

$$t = 0; \quad \forall x$$

$$C_j^{(\gamma)} = {}^* C_j^{(\gamma)} \quad j = i, v; \quad \gamma = \alpha, \beta. \quad (2)$$

Equations (1) represent the material balance of point-defects in each layer, where $C_j^{(\gamma)}$ is the concentration of the point-defect of type j in layer γ and $D_j^{(\gamma)}$ is the diffusion coefficient of the point-defect of type j in layer γ , while $K_0^{(\gamma)}$ and $R_C^{(\gamma)}$

are the production and the recombination rates of Frenkel pairs per unit volume in layer γ , respectively. $^*C_j^{(\gamma)}$ is the concentration of the point-defect of type j in layer γ at thermodynamic equilibrium, that is, the concentration value at a given temperature in absence of radiation. The reader should refer to the Nomenclature section for the significance of other symbols.

Diffusion coefficients are expressed in terms of Arrhenius form for thermally activated events as follows [41]:

$$D_j^{(\gamma)} = (a^{(\gamma)})^2 (M\nu_j^{(\gamma)}) \exp\left(-\frac{M E_j^{(\gamma)}}{k_B T}\right) \quad (3)$$

$$j = i, v; \quad \gamma = \alpha, \beta,$$

where

$$M\nu_j^{(\gamma)} = \alpha_j^{(\gamma)} \nu_D \exp\left(-\frac{M S_j^{(\gamma)}}{k_B}\right) \quad j = i, v; \quad \gamma = \alpha, \beta. \quad (4)$$

In this work, the production rate of point-defects is assumed to be time and spatially independent. It has been calculated using Transport of Ions in Matter (TRIM) [42], which is a Monte Carlo computer program that calculates the damage associated with the ion's energy loss in a material by means of efficient statistical algorithms. The recombination rate of point-defects is expressed as a second-order reaction [39]:

$$R_C^{(\gamma)} = K_{iv}^{(\gamma)} (C_i^{(\gamma)} - ^*C_i^{(\gamma)}) (C_v^{(\gamma)} - ^*C_v^{(\gamma)}) \quad \gamma = \alpha, \beta, \quad (5)$$

where the kinetic constant is given by

$$K_{iv}^{(\gamma)} = \frac{\alpha_{iv}^{(\gamma)} \Omega^{(\gamma)}}{(a^{(\gamma)})^2} (D_i^{(\gamma)} + D_v^{(\gamma)}) \quad \gamma = \alpha, \beta. \quad (6)$$

The concentrations at thermodynamic equilibrium depend on temperature according to the following equations [39]:

$$^*C_j^{(\gamma)} = \frac{1}{\Omega^{(\gamma)}} \exp\left(-\frac{F S_j^{(\gamma)}}{k_B}\right) \exp\left(-\frac{F E_j^{(\gamma)}}{k_B T}\right) \quad (7)$$

$$j = i, v; \quad \gamma = \alpha, \beta.$$

Boundary conditions for (1) (see Figure 1) should take into account the characteristics of the interfaces composing the system. Specifically, interfaces between metals α and β are modelled as variable-biased sinks considering a surface concentration of traps for interstitials, $^{\text{tot}}S_i^{(\alpha-\beta)}$, and a surface concentration of traps for vacancies, $^{\text{tot}}S_v^{(\alpha-\beta)}$. It is worth highlighting that these parameters values depend upon the metal couple α - β under investigation. The occupation probability of traps for each point-defect type is taken to be f_i and f_v , respectively. An interstitial atom adjacent to the interface is assumed to be able to enter an unoccupied interstitial trap site or to recombine with the nearest neighbor trapped vacancy, jumping there from z possible adjacent sites in the matrix.

In this work, z is set equal to 4 for any material structure [43]. Similar processes are possible for vacancies. Moreover, trapped interstitials and vacancies may recombine on the interface. Accordingly to this picture, boundary conditions at the interface between metals α and β , may be expressed as follows [43]:

$$x = \frac{L}{2}; \quad \forall t$$

$$D_j^{(\gamma)} \frac{\partial C_j^{(\gamma)}}{\partial x} = (1 - f_j + z f_k) K_j^{(\gamma)} (C_j^{(\gamma)} - ^*C_j^{(\gamma)}) \quad (8)$$

$$j = i, v; \quad k \neq j = i, v; \quad \gamma = \alpha, \beta,$$

where L is the thickness of layer γ . Boundary conditions (8) state that SIAs can reach the interface only if, in addition to a concentration gradient, there are unoccupied SIA traps ($1 - f_i > 0$) or trapped vacancies to annihilate with ($f_v > 0$). Analogous considerations can be made for vacancies. Under the assumption that the lattice is not severely distorted over the final jump region, the transfer velocities are equal to

$$K_j^{(\gamma)} = \frac{D_j^{(\gamma)}}{b^{(\gamma)}} \quad j = i, v; \quad \gamma = \alpha, \beta, \quad (9)$$

where $b^{(\gamma)}$ is the lattice spacing.

Trap occupation probabilities are obtained by solving the following balance equations:

$$\frac{df_j}{dt} = (1 - f_j) \frac{K_j^{(\alpha)}}{\text{tot}S_j^{(\alpha-\beta)}} (C_j^{(\alpha)} - ^*C_j^{(\alpha)})$$

$$+ (1 - f_j) \frac{K_j^{(\beta)}}{\text{tot}S_j^{(\alpha-\beta)}} (C_j^{(\beta)} - ^*C_j^{(\beta)})$$

$$- z f_j \frac{K_k^{(\alpha)}}{\text{tot}S_j^{(\alpha-\beta)}} (C_k^{(\alpha)} - ^*C_k^{(\alpha)}) \quad (10)$$

$$- z f_j \frac{K_k^{(\beta)}}{\text{tot}S_j^{(\alpha-\beta)}} (C_k^{(\beta)} - ^*C_k^{(\beta)}) - \frac{\alpha_s}{\text{tot}S_j^{(\alpha-\beta)}} f_j f_k$$

$$j = i, v; \quad k \neq j = i, v,$$

along with their initial condition

$$t = 0,$$

$$f_j = 0 \quad j = i, v. \quad (11)$$

Temporal evolution of trap occupation probability by the point-defect of type j depends upon fluxes to the interface arriving from both metal layers, α and β , and the recombination mechanisms occurring at the interface. Specifically, first and second terms on the right-hand side of (10) represent the flux of the point-defect of type j arriving from layers α and β , respectively, to occupy available traps at the interface.

Moreover, third and fourth terms are the flux of the point-defect of type k coming from layers α and β , respectively, to recombine with trapped point-defects of the type j . Last term quantifies the recombination of trapped SIAs with trapped vacancies. The positive or negative sign preceding the terms indicates whether the associate mechanism causes an increase or a decrease of trap occupation probability. It should be noted that (10) allow introducing interface structure features by means of trap concentration for point-defects, $^{\text{tot}}S_j^{(\alpha,\beta)}$, and the surface recombination coefficient, α_s . However, it was demonstrated in previous study [38] that point-defect annihilation at the interfaces is a diffusion-limited process and that point-defect evolutions are not affected by the α_s value. Hence, α_s has been set equal to zero in this work, which means that there is no surface recombination between trapped point-defects.

By referring to Figure 1(b), boundary conditions set can be completed by the following ones:

$$\begin{aligned} x = 0; \quad \forall t \\ \frac{\partial C_j^{(\alpha)}}{\partial x} = 0 \quad j = i, v; \end{aligned} \quad (12)$$

$$\begin{aligned} x = \frac{3L}{2}; \quad \forall t \\ \frac{\partial C_j^{(\beta)}}{\partial x} = 0 \quad j = i, v. \end{aligned} \quad (13)$$

Boundary conditions (12) express the symmetry of the system, while (13) state that the right end of layer β is treated as free surface.

The model is given by the balance equations (1) along with their initial conditions, (2), and their boundary conditions, that is, (8) in the case of the interface between metals α and β modelled as variable-biased sinks, (12) in the case of the symmetric surface of the entire system, or (13) in the case of the free surface. It allows one to describe the spatial-temporal evolution of point-defect concentrations inside layers α and β undergoing radiation.

It is worth mentioning that in this work it was assumed that point-defects produced inside a layer can not be transferred to the adjacent ones. Indeed, point-defects generated within each layer may be annihilated by recombination inside the layer or they can migrate to the interface. There, each point-defect is trapped or annihilated by surface recombination. With the aim of explaining why point-defect cannot cross the interface, let us consider, as an example, a vacancy diffusing from inside the layer toward the interface. At this point, vacancy can be trapped if unoccupied vacancy traps are available ($f_v < 1$) or can react with a trapped interstitial if present ($f_i > 0$). Even in the worst scenario, that is, no availability of both unoccupied vacancy traps and trapped interstitials at the interface, a vacancy can not cross the interface since under these conditions its flux decreases to zero (cf. (8)). It should be also considered that the point-defect concentration at the interface is always lower than the one inside the layer [38]. This means that

if a point-defect, coming, for instance, from layer α would cross the interface, the same defect should then diffuse in a countergradient manner (i.e., from low concentration regions to high concentration ones) inside the layer β . Latter event is not physically possible and then crossing the interface by point-defects is not allowed. On the other hand, metal layers influence each other's behavior through the evolution of the point-defect trap occupation probability fractions. Indeed, it can be seen (cf. (10)) that these variables behavior is affected by point-defects fluxes coming from both layers.

A change of variables was used in this work in order to obtain dimensionless and normalized equations and parameters by following the same procedure reported elsewhere [38]. Dimensionless variables and parameters, as well as scaling and reference values, are summarized in Table 1. It may be worth noting that $^s t$ can be also regarded as the characteristic time of interstitial diffusion along layer α , while the dimensionless diffusion coefficient $\delta_j^{(\gamma)}$ is defined with respect to the diffusion coefficient of SIAs in layer α . According to this change of variables, the evolution of dimensionless point-defect concentrations in layer γ as a function of the dimensionless time is described by the following equations:

$$\begin{aligned} \frac{\partial \chi_j^{(\gamma)}}{\partial \tau} - \delta_j^{(\gamma)} \frac{\partial^2 \chi_j^{(\gamma)}}{\partial \xi^2} = A^{(\gamma)} (1 - \chi_i^{(\gamma)} \chi_v^{(\gamma)}) \\ j = i, v; \quad \gamma = \alpha, \beta, \end{aligned} \quad (14)$$

along with the initial conditions

$$\begin{aligned} \tau = 0; \quad \forall \xi \\ \chi_j^{(\gamma)} = 0 \quad j = i, v; \quad \gamma = \alpha, \beta. \end{aligned} \quad (15)$$

At the interface between metals α and β modelled as variable-biased sinks, dimensionless boundary conditions may be expressed as

$$\begin{aligned} \xi = \frac{1}{3}; \quad \forall \tau \\ \delta_j^{(\gamma)} \frac{\partial \chi_j^{(\gamma)}}{\partial \xi} = \frac{3}{2} (1 - f_j + z f_k) \frac{\delta_j^{(\gamma)}}{\omega^{(\gamma)}} \chi_j^{(\gamma)} \\ j = i, v; \quad k \neq j = i, v; \quad \gamma = \alpha, \beta. \end{aligned} \quad (16)$$

The dimensionless balance equations of trap occupation probabilities appear as follows:

$$\begin{aligned} \frac{df_j}{d\tau} = E_j^{(\alpha)} \left[(1 - f_j) \frac{\delta_j^{(\alpha)}}{\omega^{(\alpha)}} \chi_j^{(\alpha)} - z f_j \frac{\delta_k^{(\alpha)}}{\omega^{(\alpha)}} \chi_k^{(\alpha)} \right] \\ + E_j^{(\beta)} \left[(1 - f_j) \frac{\delta_j^{(\beta)}}{\omega^{(\beta)}} \chi_j^{(\beta)} - z f_j \frac{\delta_k^{(\beta)}}{\omega^{(\beta)}} \chi_k^{(\beta)} \right] \\ - F_j f_j f_k \quad j = i, v; \quad k \neq j = i, v, \end{aligned} \quad (17)$$

TABLE 1: Dimensionless variables and parameters and scaling and reference values.

Name	Expression
Dimensionless point-defect concentration	$\chi_j^{(\gamma)} = \frac{C_j^{(\gamma)} - {}^r C_j^{(\gamma)}}{{}^s C_j^{(\gamma)}} \quad j = i, v; \gamma = \alpha, \beta;$
Dimensionless spatial coordinate	$\xi = \frac{x - {}^r x}{{}^s x};$
Dimensionless time	$\tau = \frac{t - {}^r t}{{}^s t};$
Dimensionless diffusion coefficient	$\delta_j^{(\gamma)} = \frac{4D_j^{(\gamma)}}{9D_i^{(\alpha)}} \quad j = i, v; \gamma = \alpha, \beta;$
Dimensionless lattice spacing	$\omega^{(\gamma)} = \frac{b^{(\gamma)}}{L} \quad \gamma = \alpha, \beta;$
—	$A^{(\gamma)} = \sqrt{\frac{L^4 K_0^{(\gamma)} \alpha_{iv}^{(\gamma)} \Omega^{(\gamma)} (D_i^{(\gamma)} + D_v^{(\gamma)})}{(a^{(\gamma)})^2 (D_i^{(\alpha)})^2}} \quad \gamma = \alpha, \beta;$
—	$E_j^{(\gamma)} = \sqrt{\frac{81L^2 K_0^{(\gamma)} (a^{(\gamma)})^2}{16 (\text{tot } S_j^{(\alpha-\beta)})^2 \alpha_{iv}^{(\gamma)} \Omega^{(\gamma)} (D_i^{(\gamma)} + D_v^{(\gamma)})}} \quad j = i, v; \gamma = \alpha, \beta;$
—	$F_j = \frac{\alpha_s L^2}{\text{tot } S_j^{(\alpha-\beta)} D_i^{(\alpha)}} \quad j = i, v;$
Reference concentration	${}^r C_j^{(\gamma)} = {}^* C_j^{(\gamma)} \quad j = i, v; \gamma = \alpha, \beta;$
Reference spatial coordinate	${}^r x = 0;$
Reference time	${}^r t = 0;$
Scaling concentration	${}^s C_j^{(\gamma)} = \sqrt{\frac{K_0^{(\gamma)}}{K_{iv}^{(\gamma)}}} \quad j = i, v; \gamma = \alpha, \beta;$
Scaling spatial coordinate	${}^s x = \frac{3L}{2};$
Scaling time	${}^s t = \frac{L^2}{D_i^{(\alpha)}};$

along with their initial conditions

$$\begin{aligned} \tau &= 0, \\ f_j &= 0 \quad j = i, v. \end{aligned} \quad (18)$$

Dimensionless boundary conditions for the symmetric surface of the entire system may be expressed as

$$\begin{aligned} \xi &= 0; \quad \forall \tau \\ \frac{\partial \chi_j^{(\alpha)}}{\partial \xi} &= 0 \quad j = i, v, \end{aligned} \quad (19)$$

while dimensionless boundary conditions represent the free surface on layer β as

$$\begin{aligned} \xi &= 1; \quad \forall \tau \\ \frac{\partial \chi_j^{(\beta)}}{\partial \xi} &= 0 \quad j = i, v. \end{aligned} \quad (20)$$

With the aim of illustrating and discussing model results, additional auxiliary quantities needed to be introduced. Specifically, let us define the average point-defect concentration in layer α and in layer β as

$$\bar{\chi}_j^{(\alpha)} = 3 \int_0^{1/3} \chi_j^{(\alpha)}(\xi) d\xi \quad j = i, v, \quad (21)$$

$$\bar{\chi}_j^{(\beta)} = \frac{3}{2} \int_{1/3}^1 \chi_j^{(\beta)}(\xi) d\xi \quad j = i, v, \quad (22)$$

respectively. The average dimensionless point-defect net-production rates are also introduced:

$$\bar{\Pi}^{(\alpha)} = 3 \int_0^{1/3} A^{(\alpha)} (1 - \chi_i^{(\alpha)} \chi_v^{(\alpha)}) d\xi, \quad (23)$$

$$\bar{\Pi}^{(\beta)} = \frac{3}{2} \int_{1/3}^1 A^{(\beta)} (1 - \chi_i^{(\beta)} \chi_v^{(\beta)}) d\xi. \quad (24)$$

The dimensionless point-defect fluxes are expressed as

$$J_j^{(\gamma)} = \delta_j^{(\gamma)} \frac{\partial \chi_j^{(\gamma)}}{\partial \xi} \quad j = i, v; \quad \gamma = \alpha, \beta. \quad (25)$$

Model equations are solved by using the commercial software COMSOL Multiphysics 3.4, along with the parameters reported in Tables 2–5.

3. Results

In what follows, copper is represented by metal α while metal β is nickel, niobium, or vanadium. Results are shown in a double-log plot (Figures 2–9) and they are obtained by solving the dimensionless version of the model illustrated in the previous section. All the results belong to the half-symmetric part of the layered system depicted in Figure 1.

Temporal profiles of average point-defect concentrations in layers α (Cu) and β (Nb, Ni, and V) are shown in Figures 2 and 3, respectively. Total irradiation time is around 90.5 s [19], which corresponds to a dimensionless time of $5 \cdot 10^9$. It can be seen in Figure 2(a) that $\bar{\chi}_i^{(\alpha)}$ constantly increases from the equilibrium concentration until $\tau \approx 0.2$. Then, average concentration of SIAs in layer α remains constant up to $\tau \approx 10^6$. This behavior can be observed for all the systems investigated. However, there is a different evolution in Cu/Ni system for later times. Indeed, in this case, $\bar{\chi}_i^{(\alpha)}$ abruptly increases to reach a higher stationary SIA average concentration with respect to Cu/V and Cu/Nb systems. Figure 2(b) shows the temporal evolution of the vacancy average concentration in layer α , $\bar{\chi}_v^{(\alpha)}$. Significant differences can be observed with respect to the behavior of $\bar{\chi}_i^{(\alpha)}$. First, it can be seen that the $\bar{\chi}_v^{(\alpha)}$ stationary state is reached at longer times ($\tau \approx 10^4$) and, secondly, the stationary value of $\bar{\chi}_v^{(\alpha)}$ is higher compared to the steady-state $\bar{\chi}_i^{(\alpha)}$ value. The overall evolution of $\bar{\chi}_v^{(\alpha)}$ appears quite similar for all the systems investigated, even if the Cu/Ni system shows a slightly lower stationary value of the vacancy average concentration.

The corresponding temporal profiles of SIA and vacancy average concentrations in layer β are shown in Figures 3(a) and 3(b), respectively. It can be seen that $\bar{\chi}_i^{(\beta)}$ reaches a stationary value at approximately the same time in Cu/V and Cu/Nb systems, while a little longer is needed for the Cu/Ni one. However, $\bar{\chi}_i^{(\beta)}$ maintains this value in V layer during the whole irradiation exposure, while an increase and a decrease in Ni and Nb layers, respectively, can be observed at longer times. Then, a new stationary state is reached in these two layers. Figure 3(b) reveals that the average concentration of vacancies in layer β , $\bar{\chi}_v^{(\beta)}$ at steady state is higher in Nb and Ni layers than in V one. It can be also observed that stationary state is reached earlier in the Cu/V system with respect to Cu/Ni and Cu/Nb ones.

In order to explain differences and similarities in the temporal evolution of point-defect average concentrations shown so far, it can be useful to investigate the advancement of all relevant phenomena concurring to produce, annihilate, and transport point-defects inside the systems.

Point-defects production rate is temporal and spatially constant (cf. (1)) but it depends upon the metal layers they are made of. Specifically, the dimensionless point-defect production rate has the following values: $0.40 \cdot 10^{-3}$, $2.88 \cdot 10^{-3}$, $0.73 \cdot 10^{-3}$, and $2.18 \cdot 10^{-3}$ for Cu, Nb, Ni, and V, respectively. On the other hand, point-defects recombination rate depends upon their concentration. This means that the net-production rate of point-defects is time and spatial dependent. The combined effects of these two phenomena are shown in Figures 4(a) and 4(b), where the temporal profiles of the average point-defect net-production rate in layer α , $\bar{\Pi}^{(\alpha)}$ and layer β , $\bar{\Pi}^{(\beta)}$ are reported, respectively. It can be clearly seen in Figure 4(a) that $\bar{\Pi}^{(\alpha)}$ does not significantly vary up to $\tau \approx 10^6$, for all the systems investigated. Then, a decrease down to a new stationary state is observed in the Cu/Ni systems. On the other hand, average point-defect net-production rate in layer α does not show any significant variation in the Cu/V and Cu/Nb systems all along the irradiation period. A different time evolution of average point-defect net-production rate may be observed in layer β . Indeed, Figure 4(b) shows that $\bar{\Pi}^{(\beta)}$ remains constant for all the systems studied only until $\tau \approx 10^4$. Then, it keeps its initial stationary value in V layer while a significant decrease occurs in Ni and Nb layers.

Besides recombination in the bulk, there is another mechanism affecting point-defect annihilation, which is point-defect flux to the interface between the two metals. Temporal profiles of point-defect fluxes from layer α and layer β to the interface between the two metals are depicted in Figures 5 and 6, respectively. SIAs diffuse much faster than vacancies (cf. Figures 5(a) and 5(b)); then SIA flux reaches its maximum earlier than vacancy one. It should be also noted that SIA and vacancy fluxes from layer α to the interface have the same value for all systems once the steady state is reached. Moreover, it can be seen that only point-defect fluxes from layer α in Cu/Ni system present differences, even though small, with respect to the other systems investigated. On the other hand, Figure 6 shows that point-defect fluxes from layer β strongly depend upon the system investigated. SIA flux from layer β to the interface (cf. Figure 6(a)), $J_i^{(\beta)}$, is much lower in the Cu/Ni system. In this system an abrupt decrease of $J_i^{(\beta)}$ at $\tau \approx 10^6$ can be also observed. Temporal profiles of $J_i^{(\beta)}$ in the other two systems are quite similar, even if a slight decrease can be seen in the Cu/Nb system at longer dimensionless times. Concerning $J_v^{(\beta)}$, it can be seen (cf. Figure 6(b)) that Cu/Ni system presents the lowest values also in this case, but there is a slight decrease instead of an abrupt one. Vice versa, the highest vacancy flux occurs in Cu/V system at any dimensionless time, even if its steady-state value is closer to the one pertaining the Cu/Nb system. In addition, $J_v^{(\beta)}$ does not show a decrease in Cu/Nb system as in the case of $J_i^{(\beta)}$.

It should be pointed out that point-defect production and bulk recombination phenomena are only dependent on the properties of the layer where they are taking place. On the other hand, point-defect flux to the interface depends upon the properties of the two adjacent layers (recalling

TABLE 2: Model parameters for copper.

Parameters	Unit	Value	Reference
a	m	$3.615 \cdot 10^{-10}$	—
b	m	$2.556 \cdot 10^{-10}$	—
${}^F E_i$	J	$4.374 \cdot 10^{-19}$	[44]
${}^F E_v$	J	$1.666 \cdot 10^{-19}$	[45]
${}^M E_i$	J	$0.131 \cdot 10^{-19}$	[44]
${}^M E_v$	J	$1.154 \cdot 10^{-19}$	[45]
k_B	JK^{-1}	$1.3806488 \cdot 10^{-23}$	—
K_0	$\text{m}^{-3} \text{s}^{-1}$	$2.05 \cdot 10^{25}$	This work
L	m	$300 \cdot 10^{-10}$	This work
${}^F S_i$	JK^{-1}	$10.257 \cdot 10^{-23}$	[46]
${}^F S_v$	JK^{-1}	$1.878 \cdot 10^{-23}$	[47]
${}^M \gamma_i$	s^{-1}	$0.20 \cdot 10^{13}$	[46]
${}^M \gamma_v$	s^{-1}	$0.76 \cdot 10^{13}$	[46]
$\text{tot } S_i^{(\text{Cu-}\beta)}$	m^{-2}	$0.13\text{--}3.20 \cdot 10^{17}$	Tables 3, 4, and 5
$\text{tot } S_v^{(\text{Cu-}\beta)}$	m^{-2}	$0.13\text{--}3.20 \cdot 10^{17}$	Tables 3, 4, and 5
T	K	573.15	This work
z	—	4	This work
α_i	—	1	[39]
α_{iv}	—	48	This work
α_s	$\text{m}^{-2} \text{s}^{-1}$	0	This work
α_v	—	1	[39]
γ_D	s^{-1}	10^{13}	[39]
Ω	m^3	$1.182 \cdot 10^{-29}$	—

TABLE 3: Model parameters for niobium.

Parameters	Unit	Value	Reference
a	m	$3.303 \cdot 10^{-10}$	—
b	m	$2.861 \cdot 10^{-10}$	—
${}^F E_i$	J	$7.370 \cdot 10^{-19}$	[48]
${}^F E_v$	J	$4.791 \cdot 10^{-19}$	[45]
${}^M E_i$	J	$0.128 \cdot 10^{-19}$	[48]
${}^M E_v$	J	$1.458 \cdot 10^{-19}$	[45]
k_B	JK^{-1}	$1.3806488 \cdot 10^{-23}$	—
K_0	$\text{m}^{-3} \text{s}^{-1}$	$1.37 \cdot 10^{25}$	This work
L	m	$300 \cdot 10^{-10}$	This work
${}^F S_i$	JK^{-1}	0	This work, [49]
${}^F S_v$	JK^{-1}	$2.899 \cdot 10^{-23}$	[50]
${}^M \gamma_i$	s^{-1}	$0.81 \cdot 10^{13}$	[48]
${}^M \gamma_v$	s^{-1}	$2.01 \cdot 10^{13}$	This work, [50]
$\text{tot } S_i^{(\text{Cu-Nb})}$	m^{-2}	$3.20 \cdot 10^{17}$	[5]
$\text{tot } S_v^{(\text{Cu-Nb})}$	m^{-2}	$3.20 \cdot 10^{17}$	[5]
T	K	573.15	This work
z	—	4	This work
α_i	—	0.16667	[39]
α_{iv}	—	144	This work
α_s	$\text{m}^{-2} \text{s}^{-1}$	0	This work
α_v	—	1	[39]
γ_D	s^{-1}	10^{13}	[39]
Ω	m^3	$1.802 \cdot 10^{-29}$	—

TABLE 4: Model parameters for nickel.

Parameters	Unit	Value	Reference
a	m	$3.520 \cdot 10^{-10}$	—
b	m	$2.489 \cdot 10^{-10}$	—
${}^F E_i$	J	$7.899 \cdot 10^{-19}$	[44]
${}^F E_v$	J	$2.195 \cdot 10^{-19}$	[45]
${}^M E_i$	J	$0.256 \cdot 10^{-19}$	[44]
${}^M E_v$	J	$2.059 \cdot 10^{-19}$	[45]
k_B	JK^{-1}	$1.3806488 \cdot 10^{-23}$	—
K_0	$\text{m}^{-3} \text{s}^{-1}$	$2.27 \cdot 10^{25}$	This work
L	m	$300 \cdot 10^{-10}$	This work
${}^F S_i$	JK^{-1}	$20.561 \cdot 10^{-23}$	This work, [51]
${}^F S_v$	JK^{-1}	$2.692 \cdot 10^{-23}$	[47]
${}^M \gamma_i$	s^{-1}	$0.79 \cdot 10^{13}$	This work, [51]
${}^M \gamma_v$	s^{-1}	$4.44 \cdot 10^{13}$	This work, [52]
$\text{tot } S_i^{\text{(Cu-Ni)}}$	m^{-2}	$0.13 \cdot 10^{17}$	[53]
$\text{tot } S_v^{\text{(Cu-Ni)}}$	m^{-2}	$0.13 \cdot 10^{17}$	[53]
T	K	573.15	This work
z	—	4	This work
α_i	—	1	[39]
α_{iv}	—	48	This work
α_s	$\text{m}^{-2} \text{s}^{-1}$	0	This work
α_v	—	1	[39]
γ_D	s^{-1}	10^{13}	[39]
Ω	m^3	$1.094 \cdot 10^{-29}$	—

TABLE 5: Model parameters for vanadium.

Parameters	Unit	Value	Reference
a	m	$3.020 \cdot 10^{-10}$	—
b	m	$2.615 \cdot 10^{-10}$	—
${}^F E_i$	J	$6.809 \cdot 10^{-19}$	[48]
${}^F E_v$	J	$4.021 \cdot 10^{-19}$	[45]
${}^M E_i$	J	$0.160 \cdot 10^{-19}$	[48]
${}^M E_v$	J	$0.993 \cdot 10^{-19}$	[45]
k_B	JK^{-1}	$1.3806488 \cdot 10^{-23}$	—
K_0	$\text{m}^{-3} \text{s}^{-1}$	$0.89 \cdot 10^{25}$	This work
L	m	$300 \cdot 10^{-10}$	This work
${}^F S_i$	JK^{-1}	0	This work
${}^F S_v$	JK^{-1}	$4.446 \cdot 10^{-23}$	[54]
${}^M \gamma_i$	s^{-1}	$1.40 \cdot 10^{13}$	[48]
${}^M \gamma_v$	s^{-1}	$1.58 \cdot 10^{13}$	This work, [55]
$\text{tot } S_i^{\text{(Cu-V)}}$	m^{-2}	$0.50 \cdot 10^{17}$	[5]
$\text{tot } S_v^{\text{(Cu-V)}}$	m^{-2}	$0.50 \cdot 10^{17}$	[5]
T	K	573.15	This work
z	—	4	This work
α_i	—	0.16667	[39]
α_{iv}	—	144	This work
α_s	$\text{m}^{-2} \text{s}^{-1}$	0	This work
α_v	—	1	[39]
γ_D	s^{-1}	10^{13}	[39]
Ω	m^3	$1.458 \cdot 10^{-29}$	—

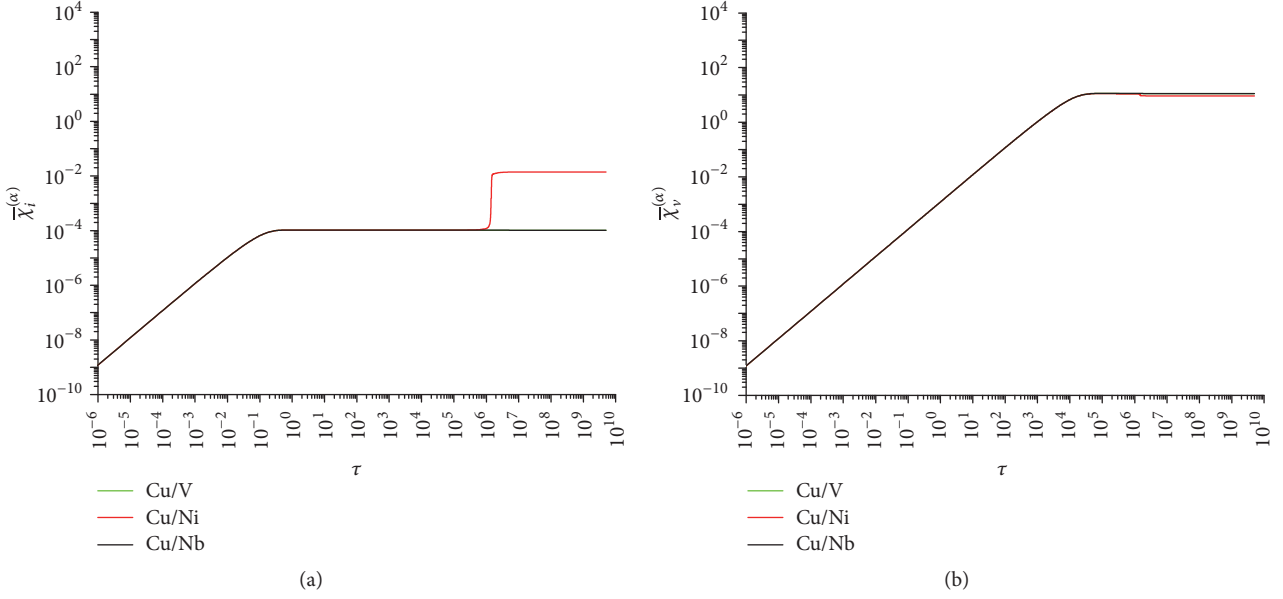


FIGURE 2: Temporal profiles of average (a) SIA and (b) vacancy concentration in layer α .

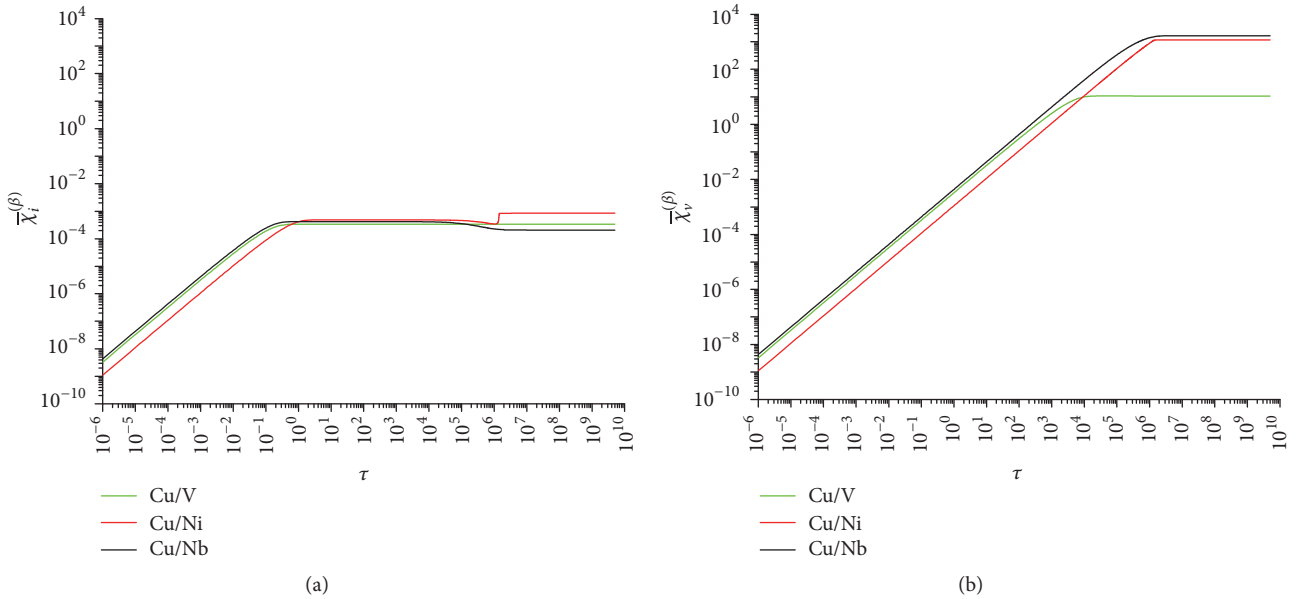


FIGURE 3: Temporal profiles of average (a) SIA and (b) vacancy concentration in layer β .

boundary condition (16)). Therefore, we should study in detail which point-defect flux the interface depends on. Besides point-defect diffusion coefficient and lattice spacing, which do not generate differences in layer α since it is the same metal (Cu) for all the systems, flux relies on point-defect concentration at the interface and trap occupation probabilities. Time evolution of point-defect concentrations at the interface located at $\xi = 1/3$ for both layers α and β is shown in Figures 7 and 8, respectively. It can be seen that time evolution of SIA (cf. Figure 7(a)) and vacancy (Figure 7(b)) interface concentration in copper layer is approximately the same for all systems investigated up to τ , equal about

10^4 . Then, we can observe an abrupt increase of the SIA concentration in the Cu/Ni system and a slight decrease of vacancy concentration for the same system. Similar behavior can be seen in Figure 8(a), where the concentration of SIAs at the interface in layer β is reported. A different evolution can be observed in Figure 8(b), where it clearly appears that the lower steady-state concentration of vacancies occurs for the Cu/V system.

Lastly, temporal profiles of trap occupation probabilities by point-defects are shown in Figure 9. Trap occupation probability by SIAs (Figure 9(a)) increases and then it reaches a stationary state for all the systems investigated. It can be

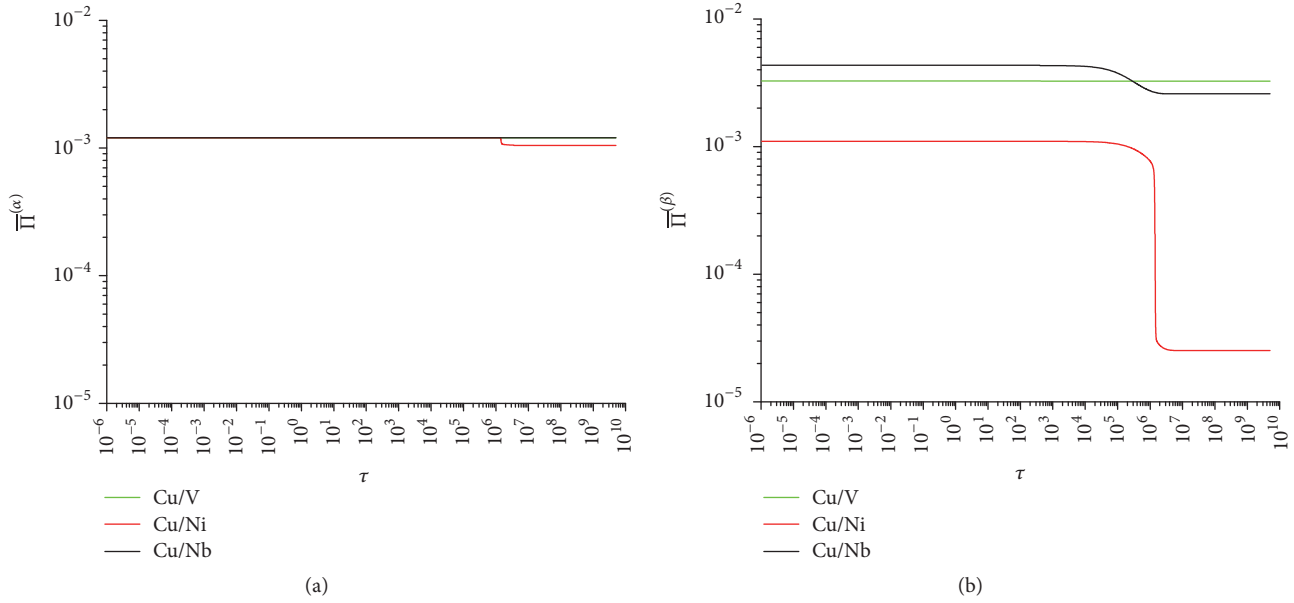


FIGURE 4: Temporal profiles of average point-defect net-production rate in (a) layer α and (b) layer β .

also seen that stationary value is higher in the Cu/Ni system and lower for the cases of Cu/Nb and Cu/V, which behave similarly, even if steady state is reached by Cu/V system sooner than by Cu/Nb one. A different behavior is shown by vacancy trap occupation probability (cf. Figure 9(b)). A similar behavior of Cu/V and Cu/Nb systems can be observed. Instead, f_v in Cu/Ni system reaches a maximum followed by a decrease down to a stationary state. It should be noted that f_i and f_v have similar values at steady state in Cu/Nb and Cu/V systems, their temporal evolution being very different than Cu/Ni coupled layers.

4. Discussion

Before starting to discuss the results shown in the previous section, it is worth recalling that thin layered systems are designed with the aim of increasing interfaces' density. This way, surface available for point-defect annihilation increases and their concentration within the system consequently decreases. Indeed, the technological goal is to maintain the concentration of SIAs and vacancies as low as possible, in order to limit clustering and then material damage induced by irradiation. Therefore, discussion of numerical simulation results should begin by commenting on and comparing point-defect concentration within the systems investigated. The behavior of the same metal Cu (layer α) is also worth highlighting, when surrounded by diverse metals β .

Temporal profiles of average SIA and vacancy concentrations in layer α and layer β are shown in Figures 2 and 3, respectively. A general comparison reveals that vacancy average concentration is typically higher than SIA one in both layers for all the systems investigated. This is a consequence of the higher diffusion rate of SIAs with respect to vacancies. Moreover, stationary state is reached by all systems investigated. It can be also seen that Cu/Nb and Cu/V systems

have a very similar behavior regarding point-defect temporal evolution in layer α (cf. Figure 2), while different profiles are shown at longer times by the Cu/Ni system. Specifically, latter system reaches a higher $\bar{\chi}_i^{(\alpha)}$ with respect to the other systems investigated, along with a lower steady-state vacancy average concentration. The mechanisms giving rise to the different behaviors underlined above are worth analyzing.

First result is as follows: higher $\bar{\chi}_i^{(\alpha)}$ should be due to higher net-production rate of SIAs and/or lower SIA flux to the α - β metals interface. Inset in Figure 5(a) confirms this explanation with respect to $J_i^{(\alpha)}$. On the other hand, lower value of $\bar{\Pi}^{(\alpha)}$ at longer time of Cu/Ni system (cf. Figure 4(a)) may be explained as an effect of the higher recombination rate generated by the higher value of $\bar{\chi}_i^{(\alpha)}$ (see (23)). The lower SIA flux shown by the Cu/Ni system is now worth enlightening. Examination of (16) reveals that $J_i^{(\alpha)}$ depends on a proportionality constant, SIA concentration at the interface, which shows a higher value according to $\bar{\chi}_i^{(\alpha)}$ (see Figure 7(a)), and trap occupation probabilities. Specifically, $J_i^{(\alpha)}$ decreases as f_i increases. Figure 9(a) indeed shows that f_i reaches its maximum value, that is, $f_i = 1$, only in the case of Cu/Ni system. This finding may then explain the lower value of $J_i^{(\alpha)}$ for this system and its peculiar behavior shown in Figure 2(a). Saturation of SIA traps at Cu/Ni interface can also clarify the lower steady-state vacancy concentration $\bar{\chi}_v^{(\alpha)}$ shown by the same system (cf. Figure 2(b)). In fact, as explained above, the higher value of $\bar{\chi}_i^{(\alpha)}$ decreases the point-defect net-production rate, which, in turn, decreases $\bar{\chi}_v^{(\alpha)}$. The lower level of this variable may also explain the lower value of $J_v^{(\alpha)}$ (cf. Figure 5(b)) through the lower value of vacancy concentration at the interface (cf. Figure 7(b)). Finally, the decrease of f_v shown in Figure 9(b) may be also elucidated as an effect of the reduced vacancy flux to the interface.

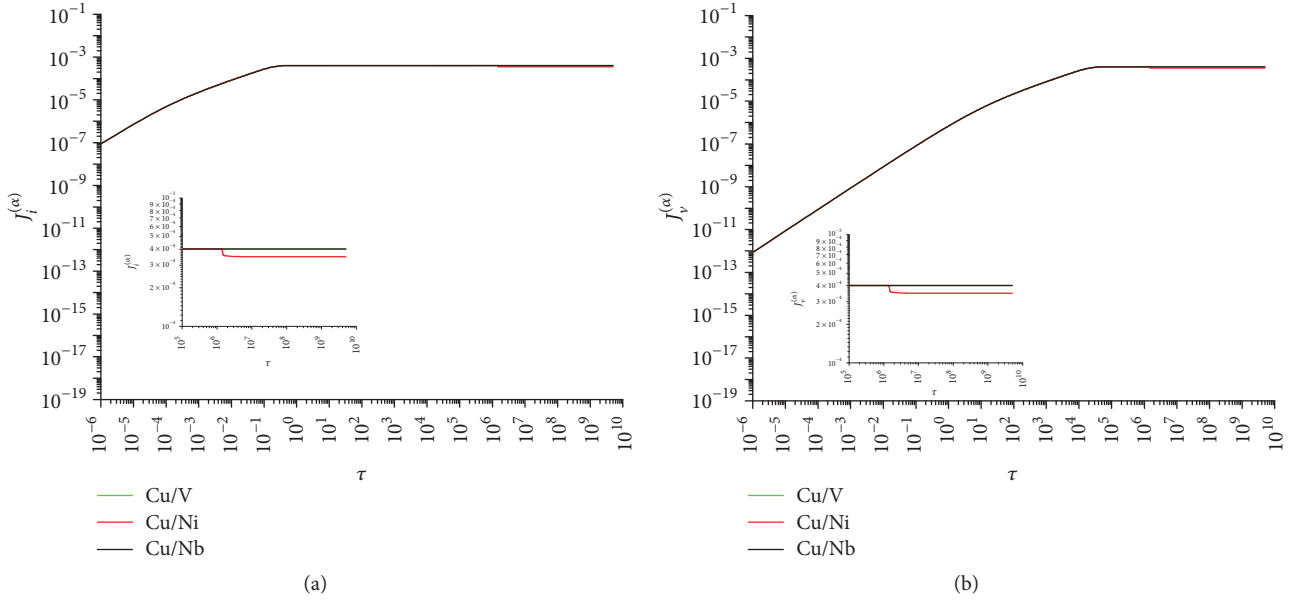


FIGURE 5: Temporal profiles of (a) SIA and (b) vacancy flux from layer α to the interface between metals α and β .

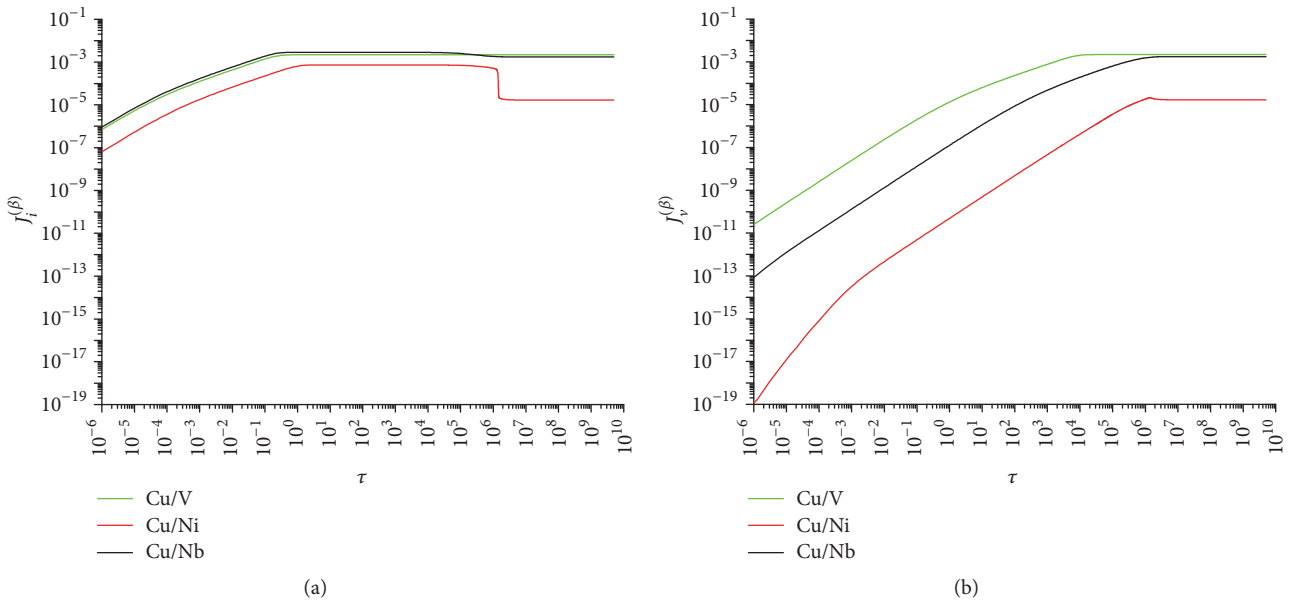


FIGURE 6: Temporal profiles of (a) SIA and (b) vacancy flux from layer β to the interface between metals α and β .

Mechanisms illustrated above are also responsible for point-defect average concentration in nickel layer (cf. Figure 3).

It was stated that Cu/Nb and Cu/V systems show a very similar behavior, being the only significant difference represented by the vacancy average concentration in vanadium layer (metal β). Specifically, Cu/V system presents a lower steady-state value of $\bar{\chi}_v^{(\beta)}$, which cannot be explained because of vacancy net-production rate. Indeed, Figure 4(b) reveals that $\bar{\Pi}^{(\beta)}$ of the Cu/V system is similar to Cu/Nb and higher than Cu/Ni even if latter ones both show a higher stationary value of $\bar{\chi}_v^{(\beta)}$. On the other hand, Figure 6(b) shows a constantly higher vacancy flux from layer β to the interface

between metals α and β in the case of Cu/V system. This finding may instead explain the lower stationary average vacancy concentration characterizing V layer.

To conclude, differences in the irradiation behavior shown by the systems investigated may be explained on the basis of both surface characteristics and bulk layer properties. Specifically, the peculiar behavior of Cu/Ni system is due to the lower value of the parameter $S_i^{\text{tot}(\text{Cu-Ni})}$ (see Tables 2–5), which induces a faster saturation of SIA traps occupation probability. Instead, higher diffusivity of vacancy in vanadium layer causes the lower stationary value of $\bar{\chi}_v^{(\beta)}$ in Cu/V system.

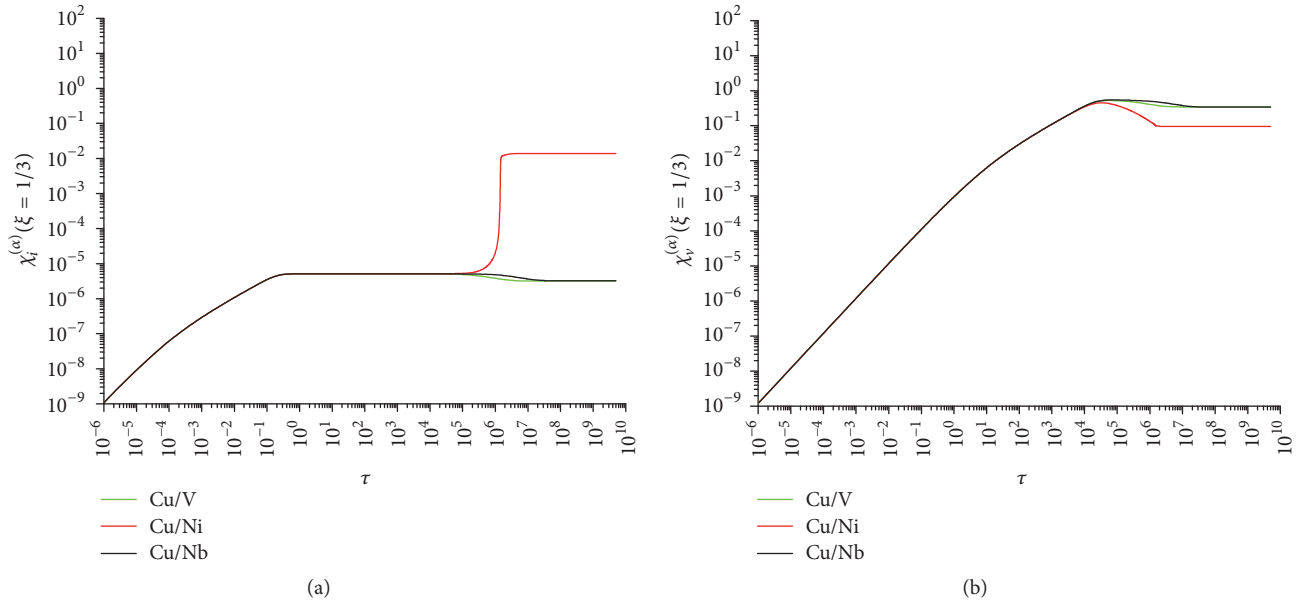


FIGURE 7: Temporal profiles of (a) SIA and (b) vacancy concentration in layer α at the interface between metals α and β .

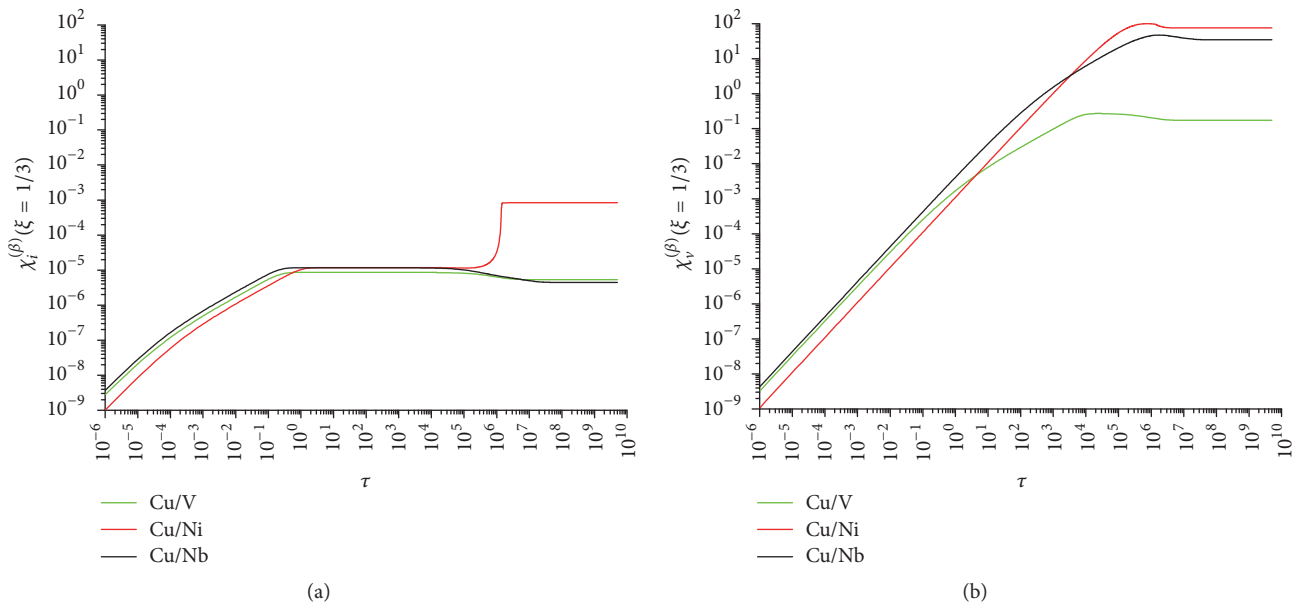


FIGURE 8: Temporal profiles of (a) SIA and (b) vacancy concentration in layer β at the interface between metals α and β .

5. Concluding Remarks

In the present work, a continuum model of point-defect evolution in multilayer composites was developed. Numerical investigation on similarities and differences between Cu/Nb, Cu/V, and Cu/Ni systems were also performed. A general comparison of model results reveals that average vacancy concentration is typically higher than SIA one in both layers for all the systems investigated. This is a consequence of the higher diffusion rate of SIAs with respect to vacancies. Stationary state is reached without saturating interface point-defect traps by all systems but Cu/Ni for the case of SIAs. It

can be also seen that Cu/Nb and Cu/V systems have a very similar behavior regarding point-defect temporal evolution in copper (layer α), while higher SIA concentration at steady state is shown therein by Cu/Ni. Moreover, Cu/V system displays the lower stationary vacancy concentration in layer β .

Differences in the irradiation behavior shown by the systems investigated may be explained on the basis of both surface characteristics and bulk layer properties. Specifically, the peculiar behavior of Cu/Ni layers is due to the lower value of the interface concentration of traps for point-defects characterizing this system, which leads to the saturation of

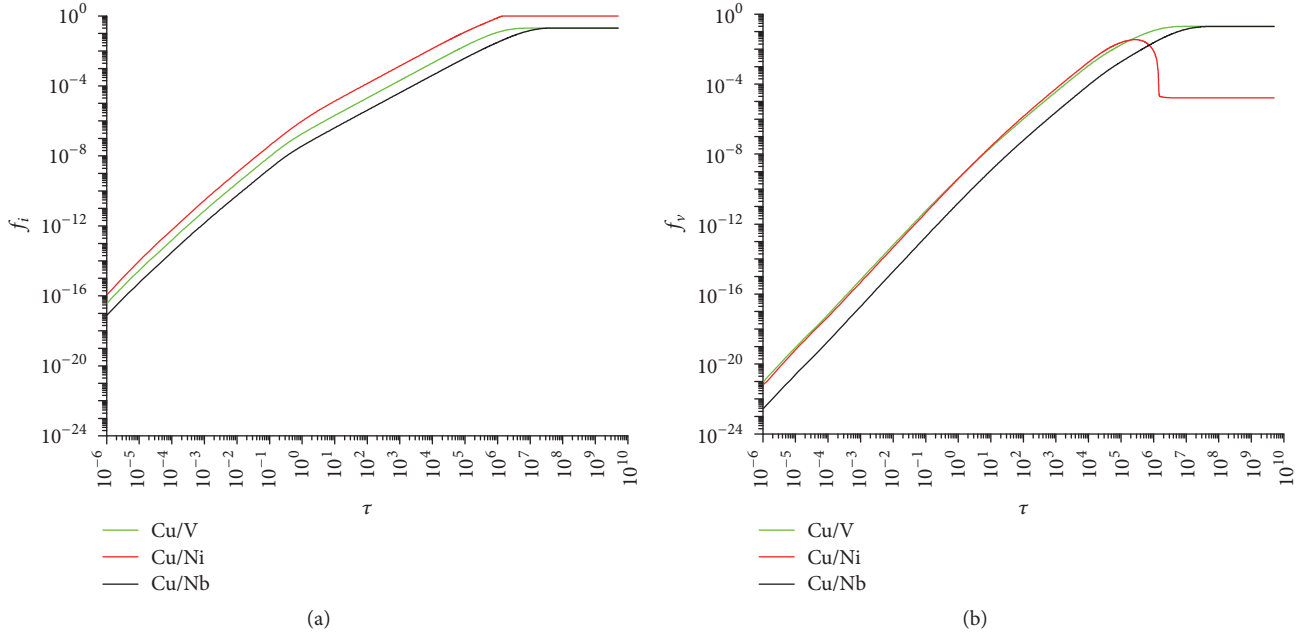


FIGURE 9: Temporal profiles of (a) SIA and (b) vacancy trap occupation probability at the interface between metals α and β .

SIA traps. Instead, higher diffusivity of vacancies in V layer causes the lower stationary value of vacancy concentration in layer β of Cu/V systems.

As a final concluding remark, model results reveal variations in interfacial Cu vacancy sink efficacy as a function of interface type. Specifically, while Cu/Nb and Cu/V interfaces are comparable in terms of point-defects absorption, Cu/Ni system results to be much less effective. These findings are qualitatively in agreement with the results reported by Mao et al. [19]. Indeed, they indicate that the average point-defect absorption probability should be highest for Cu-Nb interfaces and lowest for Cu-Ni interfaces with a moderate sink strength associated with Cu-V interfaces in between the two other systems. Work toward a quantitative comparison between model predictions and Mao et al. experimental results is along the way.

Nomenclature

- a : Lattice constant, m
- A : Dimensionless production rate of point-defects, —
- b : Lattice spacing, m
- C : Concentration of point-defects, m^{-3}
- D : Diffusivity, $\text{m}^2 \text{s}^{-1}$
- E : Dimensionless parameter of point-defect jumps from the matrix, —
- F : Dimensionless parameter of point-defect surface recombination, —
- ${}^F E$: Activation energy for formation of point-defects, J
- ${}^M E$: Activation energy for mobility of point-defects, J
- f : Trap occupation probability, —

- k_B : Boltzmann constant, J K^{-1}
- K : Transfer velocity, m s^{-1}
- K_{iv} : Recombination factor of the antidefects, $\text{m}^3 \text{s}^{-1}$
- K_0 : Production rate of point-defects, $\text{m}^{-3} \text{s}^{-1}$
- L : Layer thickness, m
- R_C : Removal rate of point-defects due to recombination, $\text{m}^{-3} \text{s}^{-1}$
- ${}^F S$: Entropy for formation of point-defects, J K^{-1}
- ${}^M S$: Entropy for mobility of point-defects, J K^{-1}
- ${}^{\text{tot}} S$: Concentration of traps for point-defects, m^{-2}
- T : Temperature, K
- t : Time, s
- x : Spatial coordinate, m
- z : Number of jumps, —.

Greek Letters

- α : Diffusion parameter of point-defects, —
- α_{iv} : Combinatorial factor, —
- α_s : Surface recombination coefficient, $\text{m}^{-2} \text{s}^{-1}$
- χ : Dimensionless concentration of point-defects, —
- δ : Dimensionless diffusivity, —
- γ_D : Debye frequency, s^{-1}
- ${}^M \nu$: Migration attempt frequency, s^{-1}
- τ : Dimensionless time, —
- ω : Dimensionless lattice spacing, —
- Ω : Atomic volume, m^3
- ξ : Dimensionless spatial coordinate, —.

Superscripts

- *: Equilibrium
- r*: Reference
- s*: Scaling
- (α): Layer of element α
- (γ): Layer of element γ
- (β): Layer of element β
- (α - β): System formed by elements α and β .

Subscripts

- i*: Self-interstitial atom
- j*: Point-defect of the type *j*
- v*: Vacancy.

Conflicts of Interest

The authors declare that the supports do not lead to any conflicts of interest. The authors also declare that there are no possible conflicts of interest related to this manuscript.

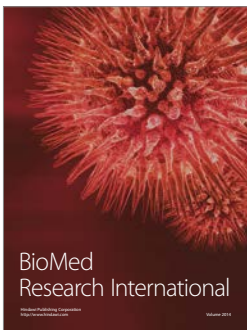
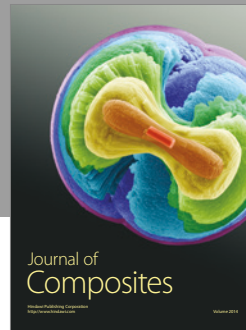
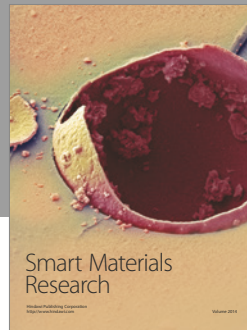
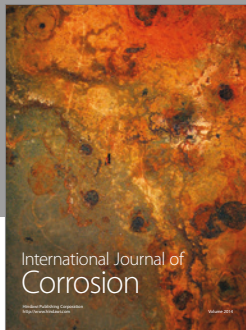
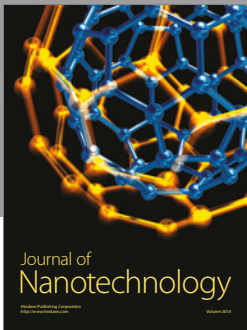
Acknowledgments

This work has been supported by the European Social Fund, Operational Programme of Castilla y León, and Junta de Castilla y León, through the Ministry of Education, as well as by the European Union Framework Programme 7, Multiscale Modelling and Materials by Design of Interface-Controlled Radiation Damage in Crystalline Materials (RADINTER-FACES) under Grant Agreement no. 263273.

References

- [1] M. J. Demkowicz, Y. Q. Wang, R. G. Hoagland, and O. Anderoglu, "Mechanisms of He escape during implantation in Cu/Nb multilayer composites," *Nuclear Instruments and Methods in Physics Research Section B: Beam Interactions with Materials and Atoms*, vol. 261, no. 1-2, pp. 524–528, 2007.
- [2] S. J. Zinkle and J. T. Busby, "Structural materials for fission & fusion energy," *Materials Today*, vol. 12, no. 11, pp. 12–19, 2009.
- [3] A. Misra, M. J. Demkowicz, X. Zhang, and R. G. Hoagland, "The radiation damage tolerance of ultra-high strength nanolayered composites," *JOM: The Journal of the Minerals, Metals & Materials Society*, vol. 59, no. 9, pp. 62–65, 2007.
- [4] S. J. Zinkle and N. M. Ghoniem, "Operating temperature windows for fusion reactor structural materials," *Fusion Engineering and Design*, vol. 51-52, pp. 55–71, 2000.
- [5] M. J. Demkowicz, A. Misra, and A. Caro, "The role of interface structure in controlling high helium concentrations," *Current Opinion in Solid State & Materials Science*, vol. 16, no. 3, pp. 101–108, 2012.
- [6] S. J. Zinkle, "Fusion materials science: overview of challenges and recent progress," *Physics of Plasmas*, vol. 12, no. 5, Article ID 058101, 2005.
- [7] M. Zhernenkov, M. S. Jablin, A. Misra et al., "Trapping of implanted He at Cu/Nb interfaces measured by neutron reflectometry," *Applied Physics Letters*, vol. 98, article 241913, 2011.
- [8] S. Mao, S. Dillon, and R. S. Averback, "The influence of Cu-Nb interfaces on local vacancy concentration in Cu," *Scripta Materialia*, vol. 69, no. 1, pp. 21–24, 2013.
- [9] S. J. Zinkle and G. S. Was, "Materials challenges in nuclear energy," *Acta Materialia*, vol. 61, no. 3, pp. 735–758, 2013.
- [10] S. W. Chee, B. Stumphy, N. Q. Vo, R. S. Averback, and P. Bellon, "Dynamic self-organization in Cu alloys under ion irradiation," *Acta Materialia*, vol. 58, no. 12, pp. 4088–4099, 2010.
- [11] H. Trinkaus and B. N. Singh, "Helium accumulation in metals during irradiation—where do we stand?" *Journal of Nuclear Materials*, vol. 323, pp. 229–242, 2003.
- [12] N. Li, N. A. Mara, Y. Q. Wang, M. Nastasi, and A. Misra, "Compressive flow behavior of Cu thin films and Cu/Nb multilayers containing nanometer-scale helium bubbles," *Scripta Materialia*, vol. 64, no. 10, pp. 974–977, 2011.
- [13] H. Ullmaier, "The influence of helium on the bulk properties of fusion reactor structural materials," *Nuclear Fusion*, vol. 24, no. 8, pp. 1039–1083, 1984.
- [14] A. Kashinath, A. Misra, and M. J. Demkowicz, "Stable storage of helium in nanoscale platelets at semicoherent interfaces," *Physical Review Letters*, vol. 110, article 086101, 2013.
- [15] N. Li, M. Nastasi, and A. Misra, "Defect structures and hardening mechanisms in high dose helium ion implanted Cu and Cu/Nb multilayer thin films," *International Journal of Plasticity*, vol. 32-33, pp. 1–16, 2012.
- [16] W. D. Wilson, C. L. Bisson, and M. I. Baskes, "Self-trapping of helium in metals," *Physical Review B: Condensed Matter and Materials Physics*, vol. 24, no. 10, pp. 5616–5624, 1981.
- [17] G. Csiszár, "Evolution of the Burgers-vector population of Cu-Nb multilayers with 7 at% He-implantation determined by X-ray diffraction," *Materials Science and Engineering: A Structural Materials: Properties, Microstructure and Processing*, vol. 609, pp. 185–194, 2014.
- [18] R. B. Adamson, W. L. Bell, and P. C. Kelly, "Neutron irradiation effects on copper at 327°C," *Journal of Nuclear Materials*, vol. 92, no. 1, pp. 149–154, 1980.
- [19] S. Mao, S. Shu, J. Zhou, R. S. Averback, and S. J. Dillon, "Quantitative comparison of sink efficiency of Cu-Nb, Cu-V and Cu-Ni interfaces for point defects," *Acta Materialia*, vol. 82, pp. 328–335, 2015.
- [20] M. Victoria, N. Baluc, C. Bailat et al., "The microstructure and associated tensile properties of irradiated fcc and bcc metals," *Journal of Nuclear Materials*, vol. 276, no. 1, pp. 114–122, 2000.
- [21] R. Escobar Galindo, A. van Veen, J. H. Evans, H. Schut, and J. T. M. De Hosson, "Protrusion formation and surface porosity development on thermally annealed helium implanted copper," *Nuclear Instruments and Methods in Physics Research Section B: Beam Interactions with Materials and Atoms*, vol. 217, no. 2, pp. 262–275, 2004.
- [22] M. Kaminsky and S. K. Das, "Correlation of blister diameter and blister skin thickness for helium-bombarded V," *Journal of Applied Physics*, vol. 49, no. 11, pp. 5673–5675, 1978.
- [23] B. Terreault, G. Ross, R. G. St-Jacques, and G. Veilleux, "Evidence that helium irradiation blisters contain high-pressure gas," *Journal of Applied Physics*, vol. 51, no. 3, pp. 1491–1493, 1980.
- [24] W. Han, M. J. Demkowicz, N. A. Mara et al., "Design of radiation tolerant materials via interface engineering," *Advanced Materials*, vol. 25, no. 48, pp. 6975–6979, 2013.
- [25] G. R. Odette, M. J. Alinger, and B. D. Wirth, "Recent developments in irradiation-resistant steels," *Annual Review of Materials Research*, vol. 38, pp. 471–503, 2008.

- [26] X. Zhang, N. Li, O. Anderoglu et al., "Nanostructured Cu/Nb multilayers subjected to helium ion-irradiation," *Nuclear Instruments and Methods in Physics Research Section B: Beam Interactions with Materials and Atoms*, vol. 261, no. 1-2, pp. 1129–1132, 2007.
- [27] P. A. Thorsen, J. B. Bilde-Sørensen, and B. N. Singh, "Bubble formation at grain boundaries in helium implanted copper," *Scripta Materialia*, vol. 51, no. 6, pp. 557–560, 2004.
- [28] L. Zhang and M. J. Demkowicz, "Morphological stability of Cu-Nb nanocomposites under high-energy collision cascades," *Applied Physics Letters*, vol. 103, no. 6, article 061604, 2013.
- [29] S. J. Zinkle, A. Horsewell, B. N. Singh, and W. F. Sommer, "Dispersoid stability in a Cu-Al₂O₃ alloy under energetic cascade damage conditions," *Journal of Nuclear Materials*, vol. 195, no. 1-2, pp. 11–16, 1992.
- [30] M. J. Demkowicz, R. G. Hoagland, and J. P. Hirth, "Interface structure and radiation damage resistance in Cu-Nb multilayer nanocomposites," *Physical Review Letters*, vol. 100, article 136102, 2008.
- [31] X. Zhang, N. Q. Vo, P. Bellon, and R. S. Averback, "Microstructural stability of nanostructured Cu-Nb-W alloys during high-temperature annealing and irradiation," *Acta Materialia*, vol. 59, no. 13, pp. 5332–5341, 2011.
- [32] Y. Chimi, A. Iwase, N. Ishikawa, M. Kobiyama, T. Inami, and S. Okuda, "Accumulation and recovery of defects in ion-irradiated nanocrystalline gold," *Journal of Nuclear Materials*, vol. 297, no. 3, pp. 355–357, 2001.
- [33] M. Ames, J. Markmann, R. Karos, A. Michels, A. Tschöpe, and R. Birringer, "Unraveling the nature of room temperature grain growth in nanocrystalline materials," *Acta Materialia*, vol. 56, no. 16, pp. 4255–4266, 2008.
- [34] T. Höchbauer, A. Misra, K. Hattar, and R. G. Hoagland, "Influence of interfaces on the storage of ion-implanted He in multilayered metallic composites," *Journal of Applied Physics*, vol. 98, article 123516, 2005.
- [35] J. S. Koehler, "Attempt to design a strong solid," *Physical Review B: Condensed Matter and Materials Physics*, vol. 2, no. 2, pp. 547–551, 1970.
- [36] S. L. Lehoczky, "Strength enhancement in thin-layered Al-Cu laminates," *Journal of Applied Physics*, vol. 49, no. 11, pp. 5479–5485, 1978.
- [37] X. Zhang, E. G. Fu, A. Misra, and M. J. Demkowicz, "Interface-enabled defect reduction in He ion irradiated metallic multilayers," *JOM: The Journal of The Minerals, Metals & Materials Society (TMS)*, vol. 62, no. 12, pp. 75–78, 2010.
- [38] S. Fadda, A. M. Locci, and F. Delogu, "Modeling of point defects annihilation in multilayered cu/nb composites under irradiation," *Advances in Materials Science and Engineering*, vol. 2016, Article ID 9435431, 17 pages, 2016.
- [39] G. S. Was, *Fundamentals of radiation materials science – Metals and alloys*, Springer, 2007.
- [40] J. Ortún-Palacios, A. M. Locci, S. Fadda, F. Delogu, and S. Cuesta-López, "Role of interface in multilayered composites under irradiation: a mathematical investigation," in *Proceedings of the Poster presentation at Spring Meeting of the European Materials Research Society*, Lille, France, May 2016.
- [41] M. J. Demkowicz, R. G. Hoagland, B. P. Uberuaga, and A. Misra, "Influence of interface sink strength on the reduction of radiation-induced defect concentrations and fluxes in materials with large interface area per unit volume," *Physical Review B: Condensed Matter and Materials Physics*, vol. 84, article 104102, 2011.
- [42] J. F. Ziegler, *Transport of Ions in Matter (TRIM)*, IBM Corp. Software, 1991.
- [43] A. D. Brailsford and R. Bullough, "The rate theory of swelling due to void growth in irradiated metals," *Journal of Nuclear Materials*, vol. 44, no. 2, pp. 121–135, 1972.
- [44] P. Zhao and Y. Shimomura, "Molecular dynamics calculations of properties of the self-interstitials in copper and nickel," *Computational Materials Science*, vol. 14, no. 1–4, pp. 84–90, 1999.
- [45] S. L. Dudarev, "Density functional theory models for radiation damage," *Annual Review of Materials Research*, vol. 43, pp. 35–61, 2013.
- [46] A. Suzuki and Y. Mishin, "Atomistic modeling of point defects and diffusion in copper grain boundaries," *Interface Science*, vol. 11, no. 1, pp. 131–148, 2003.
- [47] L. Y. Nemirovich-Danchenko, A. G. Lipnitskii, and S. E. Kul'kova, "Vacancies and their complexes in FCC metals," *Physics of the Solid State*, vol. 49, no. 6, pp. 1079–1085, 2007.
- [48] D. Finkenstadt, N. Bernstein, J. L. Feldman, M. J. Mehl, and D. A. Papaconstantopoulos, "Vibrational modes and diffusion of self-interstitial atoms in body-centered-cubic transition metals: a tight-binding molecular-dynamics study," *Physical Review B: Condensed Matter and Materials Physics*, vol. 74, no. 18, article 184118, 2006.
- [49] C. Chung-Ping, "Dislocation morphology in deformed and irradiated niobium," *Retrospective Theses and Dissertations*, Paper 5860, 1977.
- [50] F. Guethoff, B. Hennion, C. Herzig, W. Petry, H. R. Schober, and J. Trampenau, "Lattice dynamics and self-diffusion in niobium at elevated temperatures," *Journal of Physics: Condensed Matter*, vol. 6, no. 31, pp. 6211–6220, 1994.
- [51] S. Ramos De Debiaggi, M. De Koning, and A. M. Monti, "Theoretical study of the thermodynamic and kinetic properties of self-interstitials in aluminum and nickel," *Physical Review B: Condensed Matter and Materials Physics*, vol. 73, no. 10, article 104103, 2006.
- [52] S. B. Debiaggi, P. M. Decorte, and A. M. Monti, "Diffusion by vacancy mechanism in Ni, Al, and Ni₃Al: Calculation based on many-body potentials," *Physica Status Solidi (b) – Basic Solid State Physics*, vol. 195, no. 1, pp. 37–54, 1996.
- [53] S. Shao, J. Wang, A. Misra, and R. G. Hoagland, "Spiral patterns of dislocations at nodes in (111) semi-coherent FCC interfaces," *Scientific Reports*, vol. 3, article 2448, 2013.
- [54] V. Y. Chekhovskoi, V. D. Tarasov, and N. V. Grigor'eva, "Contribution of equilibrium vacancies to vanadium caloric properties," *High Temperature*, vol. 49, no. 6, pp. 826–831, 2011.
- [55] R. F. Peart, "Diffusion of V48 and Fe59 in vanadium," *Journal of Physics and Chemistry of Solids*, vol. 26, no. 12, pp. 1853–1861, 1965.



Hindawi

Submit your manuscripts at
<https://www.hindawi.com>

